

Maternal mRNA deadenylation and decay by the piRNA pathway in the early *Drosophila* embryo

Christel ROUGET¹, Catherine PAPIN¹, Anthony BOUREUX, Anne-Cécile MEUNIER, Bénédicte FRANCO, Nicolas ROBINE, Eric C. LAI, Alain PELISSON and Martine SIMONELIG

¹equal first authors

Supplementary information

Supplementary Discussion

A widespread mechanism of miRNA-mediated silencing involves deadenylation by the CCR4 deadenylase ^{1,2}. In addition, general maternal mRNA deadenylation and decay in zebrafish and *Drosophila* embryos involve miRNAs ^{3,4}. An attractive possibility could be that sequence-dependent mRNA deadenylation would require the implication of silencing RNAs in conjunction with RNA binding proteins. miRNAs involved in maternal mRNA decay during early embryogenesis are expressed zygotically. The piRNA pathway, together with Smg, might therefore allow maternal mRNA decay before the zygotic expression of miRNAs, thus contributing to the maintenance of this essential process throughout the maternal to zygotic transition in the embryo.

Supplementary Figure legends

Supplementary Figure 1: The piRNA pathway is required for *nos* mRNA deadenylation and translational repression in the bulk cytoplasm of the embryo. **(a)** PAT assays of *nos* mRNA in *armi* and *squ* mutants. Mutant females of the indicated genotypes were crossed with wild-type males. The *sop* mRNA was used as a control. PAT assay profiles using ImageJ are shown. Note that *nos* mRNA deadenylation is not affected to the same extent in the different mutants of the piRNA pathway. Deadenylation defects are weaker in *squ*, *aub* and *ago3* (Figure 1a) mutant embryos: *nos* poly(A) tails are shortened to some extent in 2-3 hour embryos from these mutants. However, the remaining poly(A) tail allows stabilization of *nos* mRNA (Figure 1b), and poly(A) tails are longer than wild-type in 3-4 hour embryos in all the tested mutants. It was recently described that the piRNA pathway components differentially impact the production of piRNAs ⁵. Strikingly, for a given piRNA pathway component, there is a good correlation between the level of its effect on germline piRNA production and on *nos* mRNA deadenylation (e.g. *squ* mutant shows a weak defect in both of these phenotypes). **(b)** *In situ* hybridizations showing that *nos* mRNA is stabilized in the bulk cytoplasm of *spn-E*, *armi* and *squ* mutant embryos. Percentages of embryos that show a defect in *nos* mRNA posterior localization in addition to *nos* stabilization in the bulk of the embryo, are from 202 and 695 embryos for *armi* and *squ* mutants, respectively. *aub* and *piwi* mutant embryos also show a defect in posterior localization of *nos* mRNA (Figure 1c), probably as a result of decreased amounts of Oskar at the posterior pole ^{6,7}. **(c)** Immunostaining of embryos with anti-Nos antibody during the first hours of embryogenesis. The ectopic expression of Nos protein was visible in the bulk of mutant embryos. **(d)** *nos* mRNA levels in 0-1 hour wild-type and mutant embryos, as quantified by RT-QPCR, showing that these levels were not significantly increased in 0-1 hour mutant embryos. The mean value of three quantifications is indicated, error bars correspond to s. d..

Supplementary Figure 2: Controls of *nos* PAT assays. **(a)** *nos* PAT assays from wild-type embryos following treatment with oligo(dT) and RNase H to degrade the poly(A) tail. After treatment, the PAT assay produces a fragment corresponding to the shorter fragment in the PAT assay without treatment, as described previously ⁸. **(b)** Examples of *nos* mRNA PAT assays from wild-type embryos and embryos from *aub* mutant females crossed with wild-type males, showing affected *nos* mRNA poly(A) tails in *aub* mutant embryos, in independent experiments. Panel 5 shows *aub* mutant PAT assays presented in Figure 1a, for comparison. Note that *aub* mutants show a weaker phenotype than

other mutants of the piRNA pathway for both piRNA production ⁵, and deadenylation and decay of *nos* mRNA (this study).

Supplementary Figure 3: The function of the piRNA pathway in *nos* mRNA deadenylation involves neither DNA repair checkpoint activation during oogenesis, nor *oskar*. (a, b) PAT assays and RT-QPCR of *nos* mRNA in *mnk aub* and *mnk armi* double mutants showing that the defects in poly(A) tail shortening and mRNA decay in *aub* and *armi* mutants are not rescued by *mnk* mutations (compare PAT assays in (a) with those in Figures 1a for *aub* mutant, and Supplementary 1a for *armi* mutant). The *sop* mRNA was used as a control. PAT assay profiles using ImageJ are shown. In (b), RT-QPCR for *aub* and *armi* mutants from Figure 1b are shown for comparison. The mean value of three quantifications is indicated, error bars correspond to s. d.. (c) *In situ* hybridizations showing that stabilization of *nos* mRNA in the bulk cytoplasm of *aub* mutant embryos is not rescued in *mnk aub* double mutant embryos. Some localization of *nos* mRNA at the posterior pole is restored in 11% of *mnk aub* double mutant embryos (n=845). (d) PAT assays of *nos* mRNA in *oskar spn-E* double mutant embryos. The defects in *nos* deadenylation in *spn-E* mutant were not rescued in the double mutant indicating that these defects do not depend on *oskar*. The *sop* mRNA was used as a control. PAT assay profiles using ImageJ are shown.

Supplementary Figure 4: Anti-Aub antibody is specific to Aub protein. Anti-Aub produces no staining in *aub* mutant embryos, showing that the cytoplasmic accumulation in discrete foci revealed with this antibody in wild-type embryos corresponds to Aub protein. (a) Confocal images of complete syncytial blastoderm embryos, anterior is to the left. (b) High magnification of syncytial blastoderm embryos showing cytoplasmic Aub in the wild-type and the lack of Aub in *aub* mutant. DAPI staining to visualize DNA (right panels).

Supplementary Figure 5: Piwi expression in embryos. Confocal images of Piwi expression in the bulk of the embryo. Syncytial blastoderm embryos at nuclear cycles 10 to 13 are shown, anterior is to the left. Piwi protein is cytoplasmic in embryos up to nuclear cycle 10. Between nuclear cycles 11 and 13, Piwi is cytoplasmic or nuclear depending on the cycle progression. An example is shown in cycle 11 where Piwi localisation changes from nuclear to cytoplasmic as a wave from the posterior to the anterior of the embryo (cycle 11). Two examples are shown for cycle 12 where Piwi is nuclear (cycle 12 upper, nuclei in prophase), then cytoplasmic (cycle 12 lower, nuclei in late prophase/early metaphase). Piwi is nuclear from cycle 13 onwards. Piwi also accumulates at the posterior pole of the embryo and is nuclear in pole cells from cycle 10 onwards ⁶. DAPI staining to visualize DNA (right panels). The specificity of anti-Piwi antibody was checked using *piwi¹* mutant embryos (bottom panels).

Supplementary Figure 6: Ago3 expression in embryos. (a) Confocal images of Ago3 expression in the bulk of the embryo (nuclear cycle 11). Ago3 is present in the cytoplasm both in the bulk of the embryo and in pole cells (right panel). There is no specific accumulation of Ago3 at the posterior pole ⁹. (b) Double immunostaining of embryos at nuclear cycles 11/12 with anti-Ago3 and anti-Smg, or anti-Ago3 and anti-CCR4, costained with DAPI (not shown). Ago3 was mostly present in the cytoplasm, diffusely distributed with accumulation in discrete foci. Ago3 partially colocalised with Smg and CCR4 both in some foci and among the diffuse pool of protein. (c) Western blots of *ago3¹/ago3³* 0-2 hour embryos revealed with anti-Ago3 showing that both *ago3* alleles produce a truncated Ago3 protein of the size expected from their molecular defects ¹⁰. α -tubulin (Tub) was used as a loading control.

Supplementary Figure 7: Controls of protein co-immunoprecipitations. (a) RNA preparations from 0-2 hour wild-type embryo extracts prepared as for co-immunoprecipitations, in the absence (-) or in the presence (+) of 0.1 μ g/ μ l RNase A, showing degradation of RNA in the presence of RNase A. (b) Immunoprecipitation of GFP-Aub in 0-2 hour embryos from *nosGal4:VP16/UASp-GFP-Aub* females crossed with wild-type males, in the presence of 0.1 μ g/ μ l RNase A (mock IP: mouse anti-HA) showing that Piwi is not co-precipitated (left panel). Immunoprecipitation of Aub in 0-2 hour wild-

type embryos in the presence of 0.1 μ g/ μ l RNase A (mock IP: mouse anti-HA) showing that Piwi is not co-precipitated (right panel). (c) Co-immunoprecipitation of CCR4, Aub and Ago3 with Smg in 0-2 hour wild-type embryo extracts in the presence of 0.1 μ g/ μ l RNase A and 7 units of micrococcal nuclease which degrades poly(A) (mock IP: guinea pig pre-immune serum), showing that the co-immunoprecipitation is maintained in the absence of RNA and poly(A).

Supplementary Figure 8: piRNAs from *roo* and *412* transposons complementary to *nos* 3'-UTR. (a) piRNAs complementary to *nos* 3'-UTR were identified using Blast and piRNA data sets from 0-1 hour and 0-2 hour embryos. Both piRNA families showing complementarity to *nos* 3'-UTR are presented. Complementary nucleotides are in bold. The piRNAs are in the sense strand of *412* and in the antisense strand of *roo*. (b) Potential annealing with *nos* 3'-UTR of a representative piRNA per family is shown. Coordinates are from *nos* 3'-UTR, with 1 corresponding to the first nt after the stop codon. The 15 nt and 11 nt deleted in the *nos*(Δ *pi412*) and *nos*(Δ *piroo*) transgenes are indicated with a line.

Supplementary Figure 9: Controls of primers used in PAT assays. (a) Schematic representation of *nos* 3'-UTR, primers used in (b) and (c) are represented by arrows. The dT-anchor primer is used for the reverse transcription reaction. (b) PAT assays of *nos* mRNA in embryos from females of the indicated genotypes crossed with wild-type males. *nos*(Δ) transgenes are *nos* genomic transgenes in which different regions of the 3'-UTR have been deleted. *nos*^{BN} mutant does not produce *nos* mRNA. The *nos* sequence amplified in PAT assays with primer 2 is 150 nt long without poly(A), whereas the *nos* sequence amplified in PAT assays from *nos*(Δ 3) with primer 1 is 99 nt long without poly(A). Note that the shorter PCR fragments in these PAT assays are 30 nt longer than these sizes due to the length of the dT-anchor primer. Both kinds of PAT assays are shown here on the same gel. (c) PAT assays of *nos* mRNA in wild-type embryos using primer 1 showing a normal profile of *nos* mRNA deadenylation; the *nos* sequence amplified in these PAT assays is 328 nt long without poly(A). The primers used for the PCR are indicated below the gels in (b) and (c).

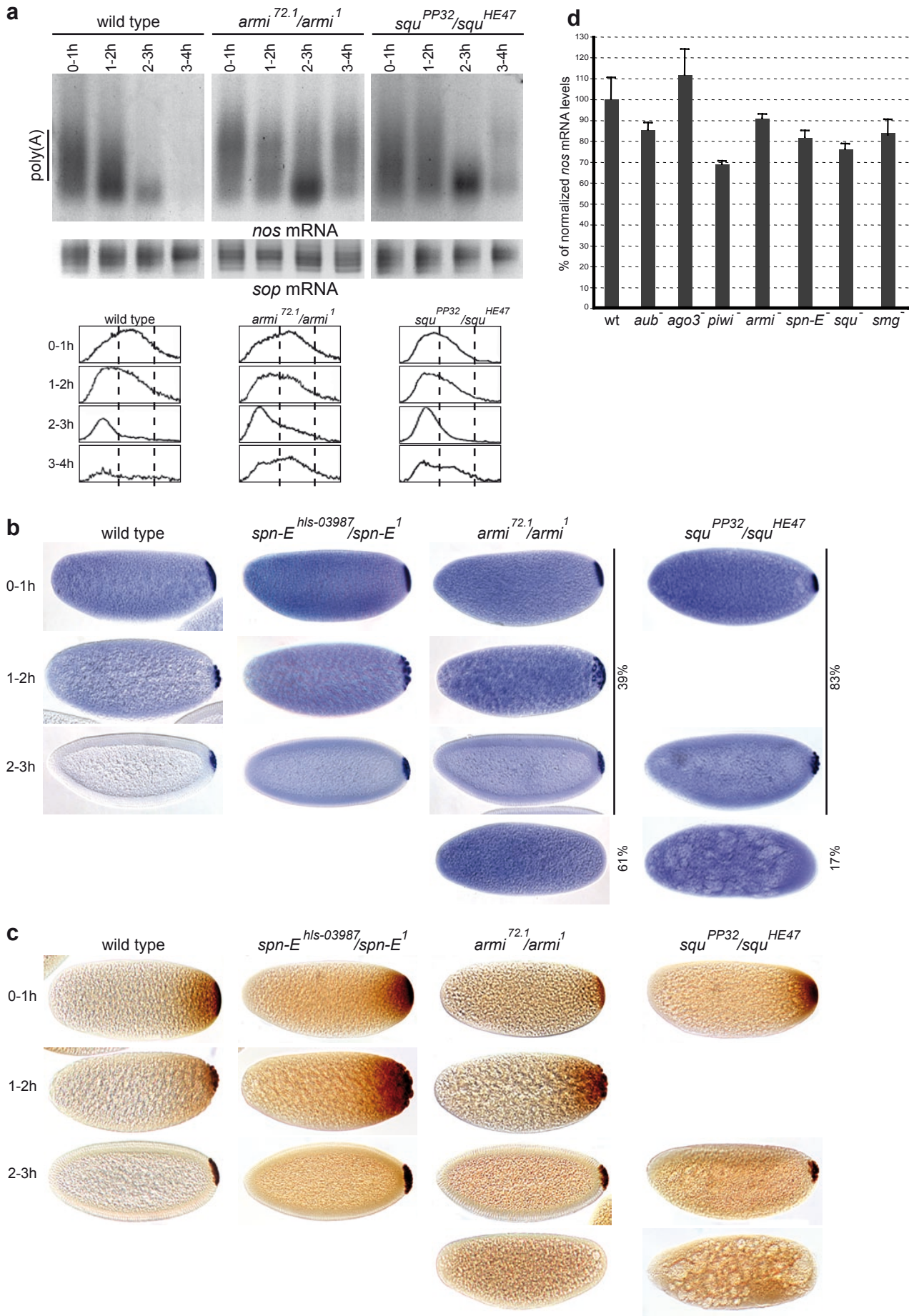
Supplementary Figure 10: Model of protein-protein and RNA-protein interactions in the complex mediating *nos* mRNA deadenylation in the embryo. Part of *nos* coding sequence is represented (bold line). The *nos* 3'-UTR is schematized by a thin line. The CCR4 deadenylation complex is composed of seven proteins (in black) ¹¹. Smg interacts with the deadenylation complex, potentially through the CAF1 subunit ¹² and recruits the complex via the SRE localized in the 5' region of the 3'-UTR. Retrotransposon piRNAs complementary to *nos* 3'-UTR assemble with Aub and Ago3 and guide their interaction with the 3' region of *nos* 3'-UTR. Note that potential secondary structures in *nos* 3'-UTR are not represented. Aub and Ago3 interacting either directly or through additional proteins with the deadenylation complex help in stabilizing the complex onto *nos* mRNA. The spacing between the SREs and the piRNA target sites can vary to some extent without affecting the regulation, as a 219-nt deletion in the *nos*(Δ 1) transgene does not affect deadenylation.

Supplementary Figure 11: Role of the piRNA pathway in the deadenylation of maternal unstable mRNAs. (a) PAT assays performed for four maternal unstable mRNAs ¹³ showing a reduced deadenylation in *aub* and *piwi* mutant embryos. Note that the stability of cellular mRNAs has been found to be unaffected in piRNA pathway mutants when analysed in ovaries ^{14,15}, consistent with the fact that mRNAs are more stable in ovaries than in embryos ¹⁶. (b) PAT assays of *oskar* and *me31B* mRNAs in *smg* mutant embryos showing that deadenylation of these mRNAs is *smg*-dependent. Decay of *hsp83* and *grapes* mRNAs was described previously as being *smg*-dependent ¹³. PAT assay profiles using ImageJ are shown. (c) piRNAs complementary to 3'-UTR of the mRNAs analysed in (a) identified using Blast (NCBI Blast with an E value of 100 and a 14-nt match). Coordinates are from each 3'-UTR, with 1 corresponding to the first nt after the stop codon.

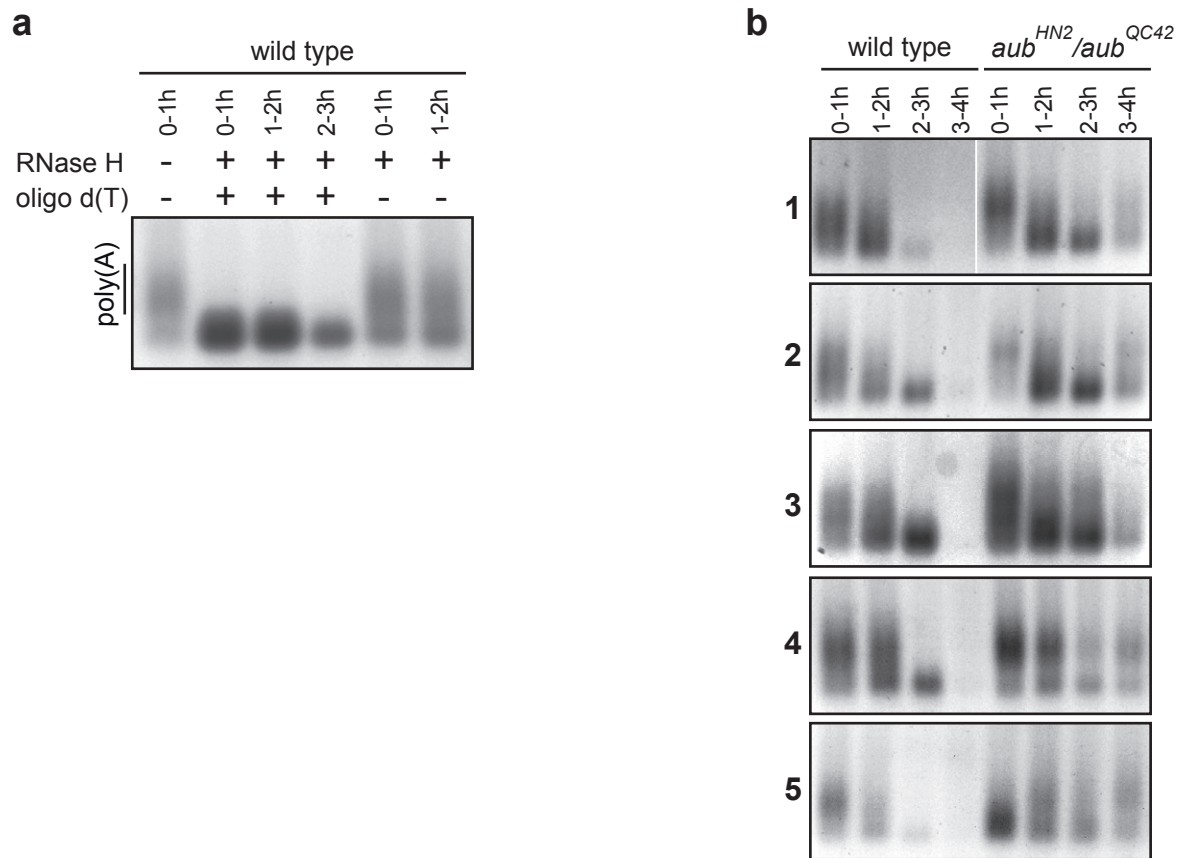
Supplementary Figure 12: Profiles of PAT assays shown in Figure 1a (a), Figure 4c (b) and Figure 4f (c), using ImageJ.

References

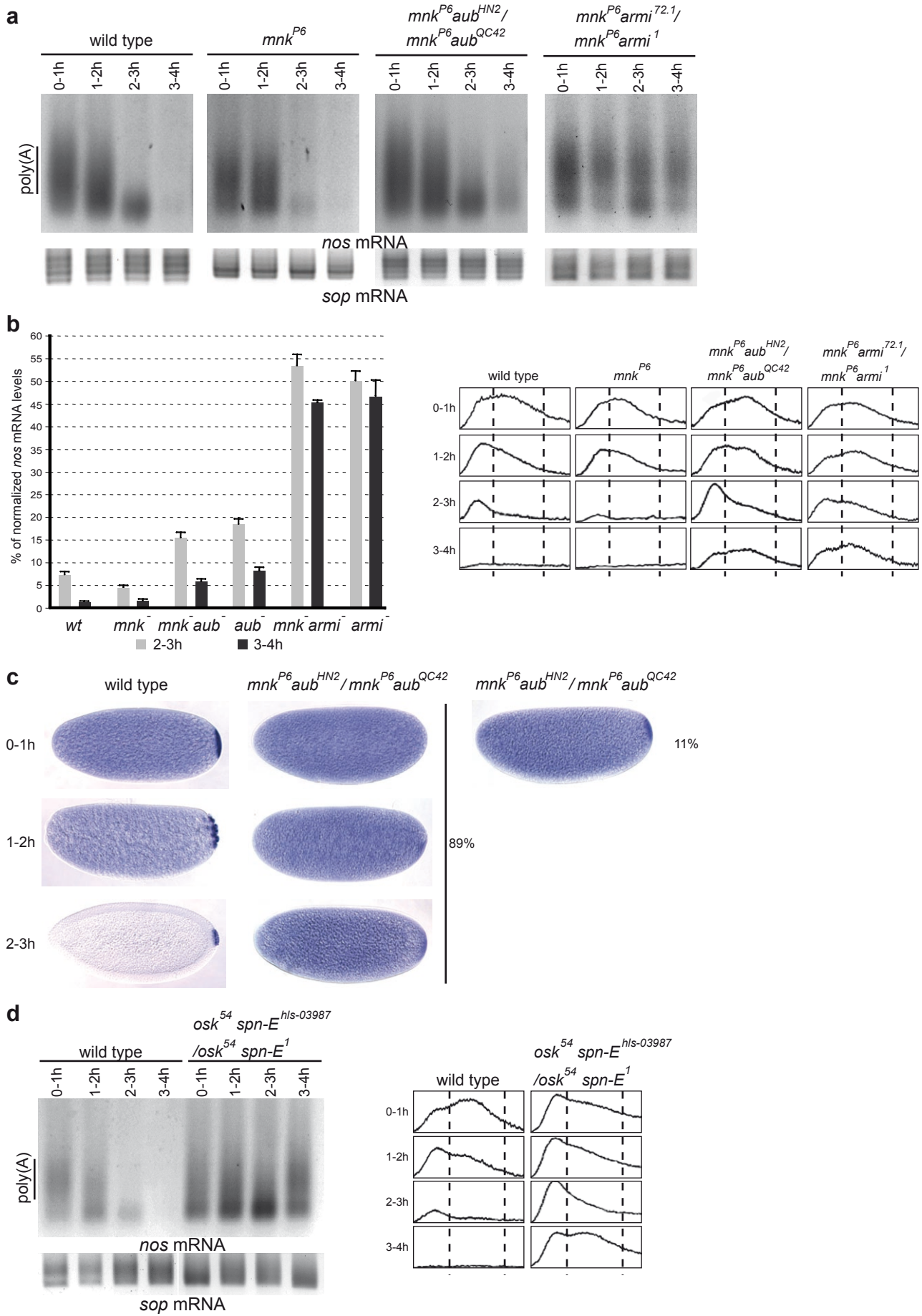
1. Eulalio, A. et al. Deadenylation is a widespread effect of miRNA regulation. *Rna* **15**, 21-32 (2009).
2. Fabian, M. R. et al. Mammalian miRNA RISC recruits CAF1 and PABP to affect PABP-dependent deadenylation. *Mol Cell* **35**, 868-80 (2009).
3. Giraldez, A. J. et al. Zebrafish MiR-430 Promotes Deadenylation and Clearance of Maternal mRNAs. *Science* (2006).
4. Bushati, N., Stark, A., Brennecke, J. & Cohen, S. M. Temporal reciprocity of miRNAs and their targets during the maternal-to-zygotic transition in *Drosophila*. *Curr Biol* **18**, 501-6 (2008).
5. Malone, C. D. et al. Specialized piRNA pathways act in germline and somatic tissues of the *Drosophila* ovary. *Cell* **137**, 522-35 (2009).
6. Megosh, H. B., Cox, D. N., Campbell, C. & Lin, H. The role of PIWI and the miRNA machinery in *Drosophila* germline determination. *Curr Biol* **16**, 1884-94 (2006).
7. Wilson, J. E., Connell, J. E. & Macdonald, P. M. aubergine enhances oskar translation in the *Drosophila* ovary. *Development* **122**, 1631-9 (1996).
8. Rouget, C., Papin, C. & Mandart, E. Cytoplasmic CstF-77 protein belongs to a masking complex with cytoplasmic polyadenylation element-binding protein in *Xenopus* oocytes. *J Biol Chem* **281**, 28687-98 (2006).
9. Brennecke, J. et al. An epigenetic role for maternally inherited piRNAs in transposon silencing. *Science* **322**, 1387-92 (2008).
10. Li, C. et al. Collapse of germline piRNAs in the absence of Argonaute3 reveals somatic piRNAs in flies. *Cell* **137**, 509-21 (2009).
11. Temme, C., Zaessinger, S., Meyer, S., Simonelig, M. & Wahle, E. A complex containing the CCR4 and CAF1 proteins is involved in mRNA deadenylation in *Drosophila*. *EMBO J.* **23**, 2862-2871 (2004).
12. Semotok, J. L. et al. Smaug recruits the CCR4/POP2/NOT deadenylase complex to trigger maternal transcript localization in the early *Drosophila* embryo. *Curr Biol* **15**, 284-94 (2005).
13. Tadros, W. et al. SMAUG is a major regulator of maternal mRNA destabilization in *Drosophila* and its translation is activated by the PAN GU kinase. *Dev Cell* **12**, 143-55 (2007).
14. Klattenhoff, C. et al. The *Drosophila* HP1 homolog Rhino is required for transposon silencing and piRNA production by dual-strand clusters. *Cell* **138**, 1137-49 (2009).
15. Lim, A. K., Tao, L. & Kai, T. piRNAs mediate posttranscriptional retroelement silencing and localization to pi-bodies in the *Drosophila* germline. *J Cell Biol* **186**, 333-42 (2009).
16. Benoit, P., Papin, C., Kwak, J. E., Wickens, M. & Simonelig, M. PAP- and GLD-2-type poly(A) polymerases are required sequentially in cytoplasmic polyadenylation and oogenesis in *Drosophila*. *Development* **135**, 1969-79 (2008).



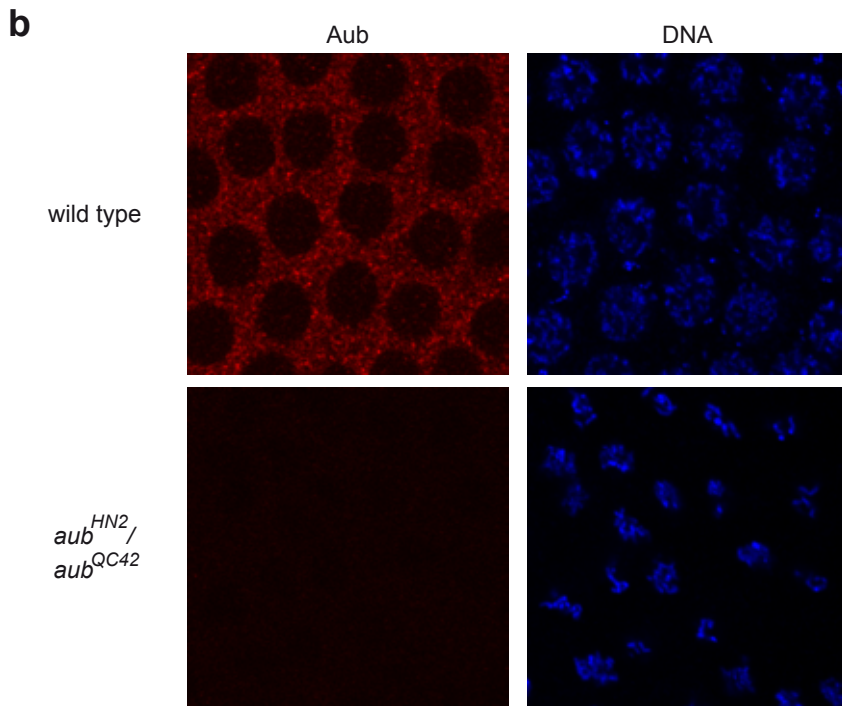
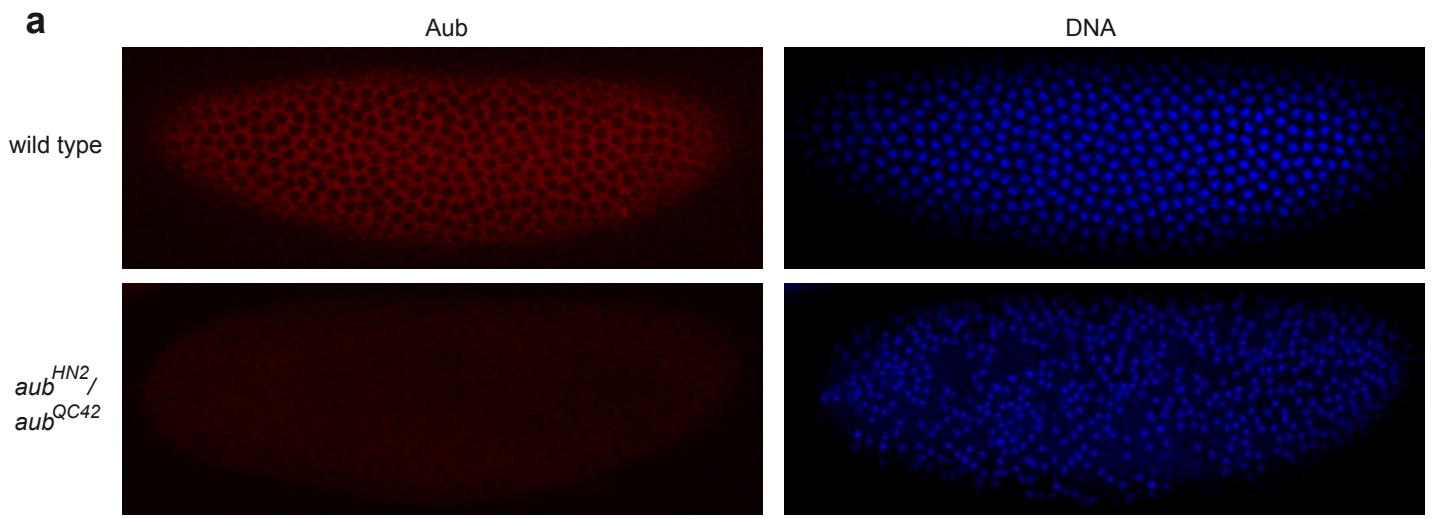
Supplementary Figure 1



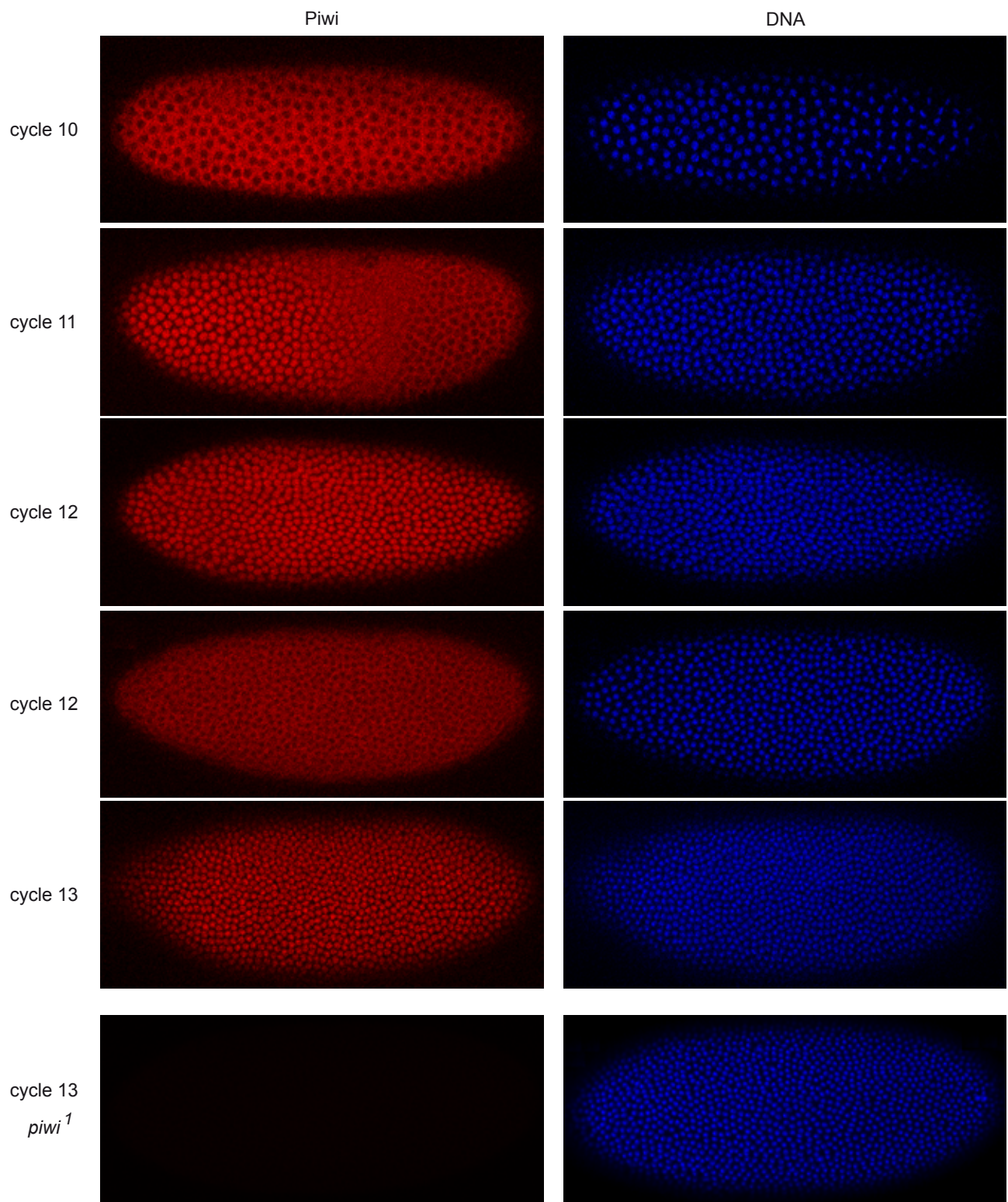
Supplementary Figure 2



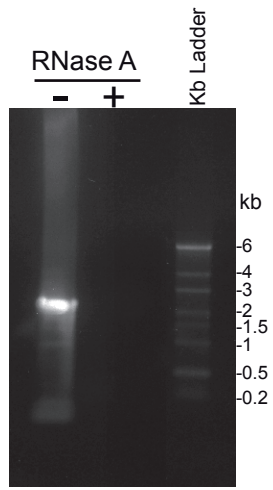
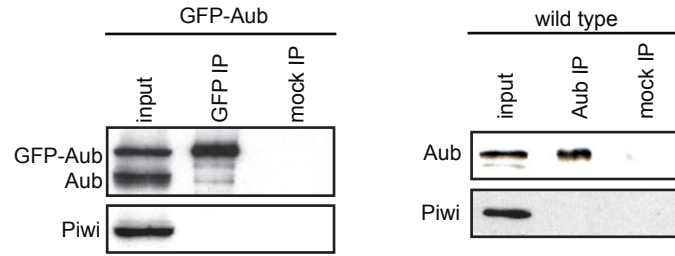
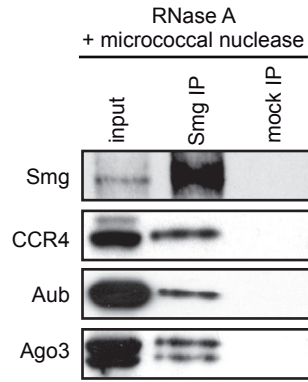
Supplementary Figure 3



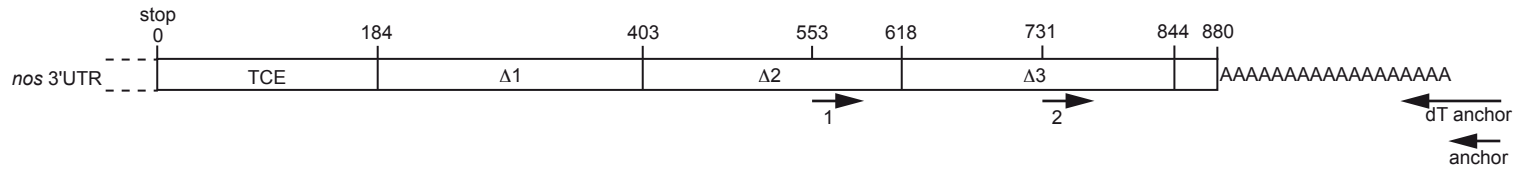
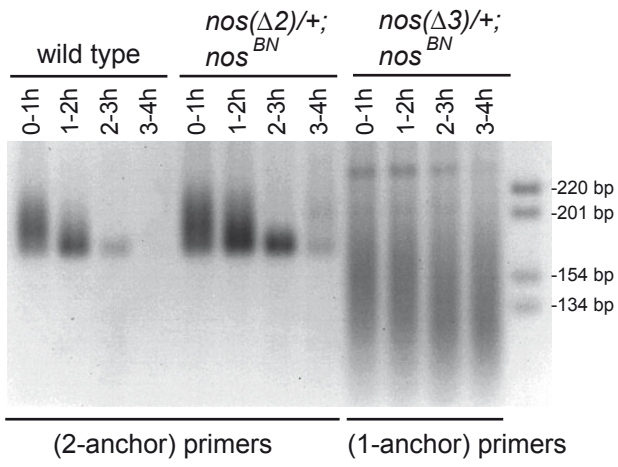
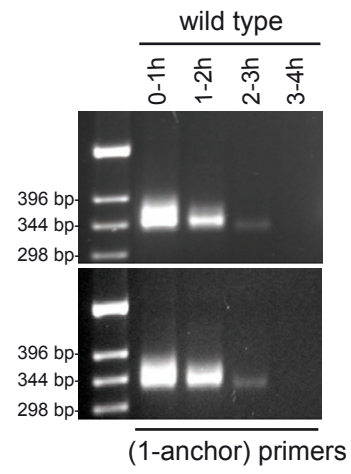
Supplementary Figure 4



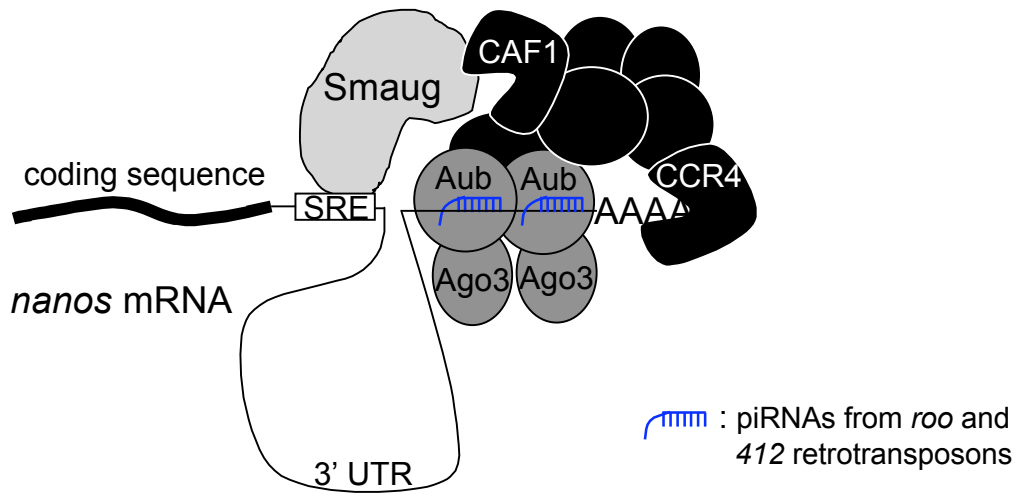
Supplementary Figure 5

a**b****c**

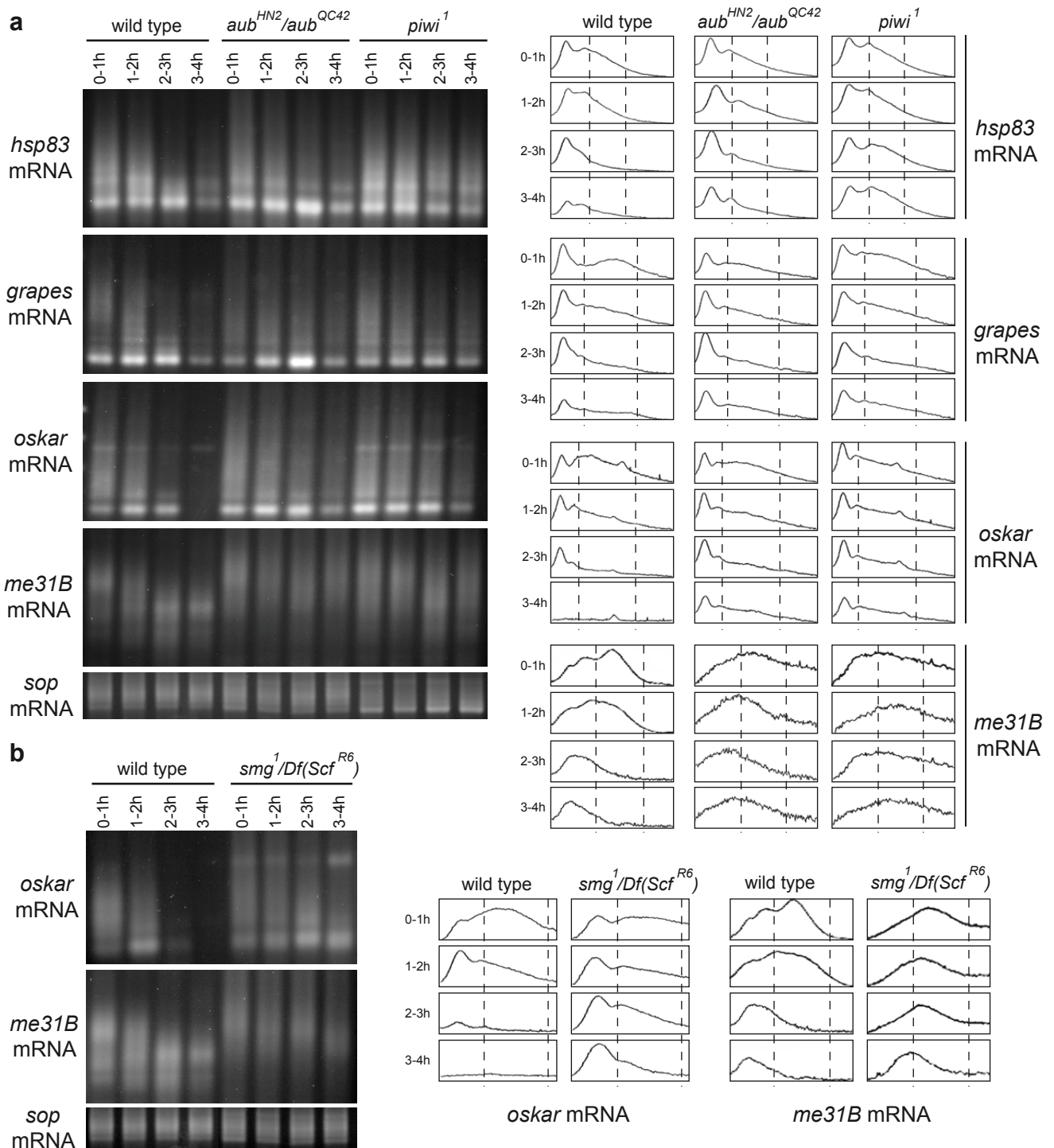
Supplementary Figure 7

a**b****c**

Supplementary Figure 9



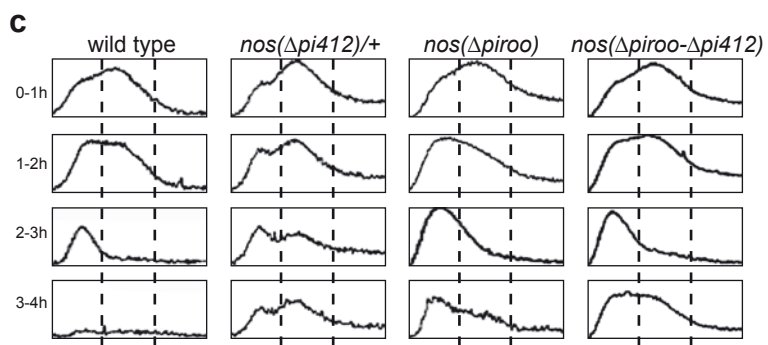
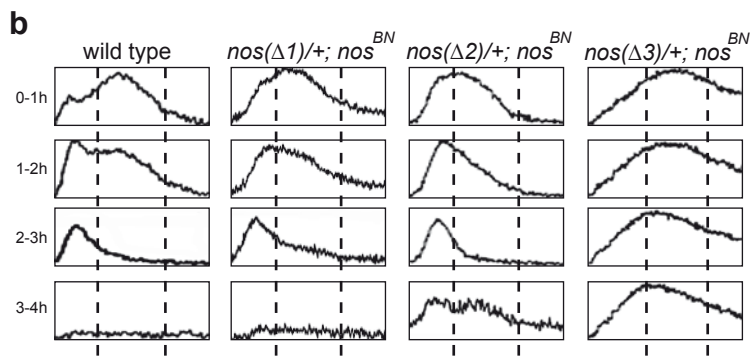
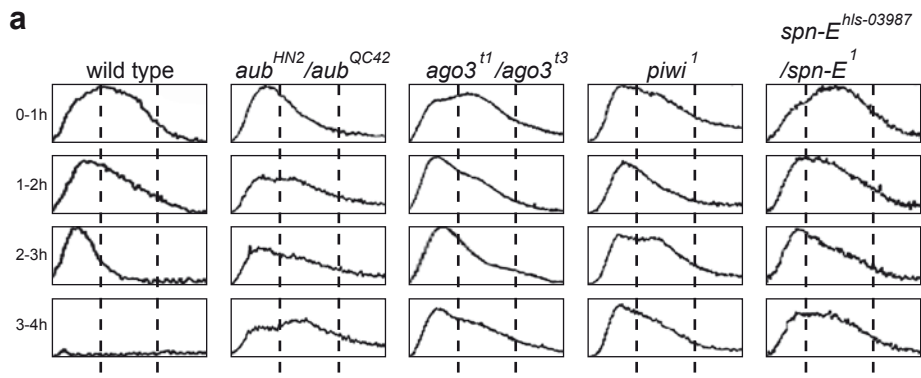
Supplementary Figure 10



c

target mRNA	targeted region	transposon of origin	piRNA occurrence	annealing length
<i>hsp83</i>	246-259	roo	1636	14
	375-388	rover	58	14
	163-176	McClintock	52	14
<i>grapes</i>	199-213	HeT-A	108	15
<i>oskar</i>	82-97	TART-B	225	16
	136-150	Cr1a	68	15
<i>me31B</i>	54-67	297	874	14
	93-106	U chromatin	316	14

Supplementary Figure 11



Supplementary Figure 12